Journal of Organometallic Chemistry, 394 (1990) 121–143
Elsevier Sequoia S.A., Lausanne
JOM 21128

The ketenylidene route to mixed-metal carbide clusters: $[MnRu_3C(CO)_{13}]^-$, $[MnOs_3C(CO)_{13}]^-$, $[Cr_2Ru_3C(CO)_{16}]^{2-}$, $[Mo_2Ru_3C(CO)_{16}]^{2-}$, $[Rh_3Ru_3C(CO)_{15}]^-$, $[Ni_3Ru_3C(CO)_{13}]^{2-}$ and $[Co_3Ru_3C(CO)_{15}]^-$ *

Michael P. Jensen, William Henderson, Dean H. Johnston, Michal Sabat and Duward F. Shriver *

Department of Chemistry, Northwestern University, Evanston, IL 60208-3113 (U.S.A.)

(Received March 12th, 1990)

Abstract

Redox-condensation reactions between the ketenylidene clusters $[M_3(CO)_9CCO]^{2-}$ (M = Ru, Os) and electrophilic transition-metal reagents provide a convenient route to the new carbido clusters $[PPN][MnRu_3C(CO)_{13}]$, $[PPN][MnOs_3C(CO)_{13}]$, $[PPN]_2[Cr_2Ru_3C(CO)_{16}]$, $[PPN]_2[Mo_2Ru_3C(CO)_{16}]$, $[PPN][Rh_3Ru_3C(CO)_{15}]$, $[PPN]_2[Ni_3Ru_3C(CO)_{13}]$, and $[PPN][Co_3Ru_3C(CO)_{15}]$. These clusters have been characterized by elemental analysis, IR and variable-temperature ^{13}C NMR spectroscopy, and, in the case of $[PPN][MnOs_3C(CO)_{13}]$ and $[PPN]_2[Ni_3Ru_3C(CO)_{13}]$ by single-crystal X-ray diffraction studies. The $[MnOs_3C(CO)_{13}]^-$ cluster consists of a butterfly array of metal atoms with the manganese occupying a hinge position. The structure of the $[Ni_3Ru_3C(CO)_{13}]^{2-}$ is a distorted (opened) octahedron of metal atoms, with the three ruthenium atoms forming one closed face of the octahedron, and the carbide ligand occupying an interstitial site. ^{13}C NMR data indicate the octahedron closes in solution. For $[PPN][MnRu_3C(CO)_{13}]$ and $[PPN][MnOs_3C(CO)_{13}]$, the carbide ligands show variable temperature NMR behavior, which is best interpreted in terms of a two-bond spin–spin coupling of the carbide to the two *endo* carbonyls on the wingtip Ru or Os atoms. A similar two-bond coupling process may possibly also be operating in the $[Cr_2Ru_3C(CO)_{16}]^{2-}$ cluster.

---

* Dedicated to Professor F.G.A. Stone on the occasion of his 65th birthday.

0022-328X/90/$03.50

Introduction

Transition metal carbide clusters continue to attract interest as a class of compounds which contain a carbon atom bonded only to metal atoms [1]. Since the first carbide cluster, $Fe_5C(CO)_{15}$ was identified crystallographically in 1962 [2], a large number of carbido carbonyl clusters have been synthesized [1,3,4]. Carbide ligands are not, however, limited to low valent carbonyl containing clusters. Indeed, the ubiquity of the carbide ligand in metal cluster chemistry has recently been demonstrated by the syntheses of alkoxo-carbido clusters $[W_4(C)(X)(O^iPr)_{12}]$ (X = O, NMe) [5], and a range of solid-state carbide clusters containing halide ligands [6].

We have shown that the iron ketenylidene cluster $[Fe_3(CO)_9(CCO)]^{2-}$ is a versatile precursor for the facile high-yield syntheses of a wide range of mixed-metal carbide clusters [7]. These reactions, with electrophilic transition metal fragments, proceed by redox-condensation processes [8], and have led to the isolation of FeCr, FeW, FeMn, FeNi and FeRh carbido carbonyl clusters. This methodology was first employed to prepare hexanuclear carbides from $[Fe_5C(CO)_{14}]^{2-}$ [9]. Recent work by Stone and co-workers [10] demonstrates that cluster building may also be accomplished via reaction of the neutral ketenylidene cluster $H_2Os_3(CO)_9(CCO)$ with the nucleophilic platinum complex $[Pt(C_2H_4)_2(PCy_3)]$ (Cy = *cyclo*-C_6H_{11}) to afford the carbido clusters $H_2Os_3PtC(CO)_{10}(PCy_3)$ and $H_2Os_3Pt_2C(CO)_{10}(PCy_3)_2$. Similarly, $Co_3(CO)_9CH$ reacts with $Pt(C_2H_4)_2(P^iPr_3)$ to yield $[Co_3Pt_2C(\mu\text{-}H)(CO)_9(P^iPr_3)]$ and $[Co_3Pt_3C(\mu\text{-}H)(CO)_9(P^iPr_3)_2]$.

In addition to $[Fe_3(CO)_9(CCO)]^{2-}$, we have developed syntheses for the related ruthenium [11] and osmium [12] ketenylidenes. In the research reported here we investigated the use of these ketenylidene clusters in the synthesis of mixed-metal ruthenium and osmium carbido carbonyl clusters. Although an extensive number of homometallic ruthenium and osmium carbido carbonyl clusters have been described [1,3,13], relatively few mixed-metal ruthenium or osmium carbido carbonyl clusters have been reported. Redox condensation reactions between $[Ru_5C(CO)_{14}]^{2-}$ and $M(CO)_3L_3$ (M = Cr, Mo, W) [14] have yielded the hexanuclear mixed-metal clusters $[MRu_5C(CO)_{17}]^{2-}$, and as mentioned earlier, mixed-metal osmium-platinum carbido clusters may be formed from the neutral ketenylidene $H_2Os_3(CO)_9(CCO)$ [10]. A mixed tetranuclear Ru_2Pt_2 carbido cluster has also been prepared [15]. Finally, a number of gold(I), copper(I), mercury(II) and thallium(III) derivatives of ruthenium and osmium carbido carbonyl clusters are known [1,3].

In this paper, we report that the ruthenium and osmium ketenylidene clusters $[M_3(CO)_9(CCO)]^{2-}$ may be employed in redox-condensation reactions to afford high yields of tetra-, penta-, and hexanuclear MnRu, CrRu, MoRu, CoRu, RhRu, NiRu and MnOs clusters.

Experimental

General procedures and materials

All compounds described in this work are somewhat air-sensitive. Therefore, manipulations were carried out under an atmosphere of dried and deoxygenated nitrogen, employing standard Schlenk and syringe techniques [16]. Solids were manipulated in a Vacuum Atmospheres glovebox equipped with a recirculator and Dri-Train system. Pentane was stored over concentrated H_2SO_4 prior to drying.

Solvents were refluxed over and then distilled from appropriate drying agents under nitrogen prior to use (THF and Et_2O from Na/benzophenone ketyl; 2-propanol from Mg/I_2; acetone and pentane from 4Å sieves). NMR solvents were freeze-pump-thaw degassed twice and then vacuum-distilled from appropriate drying agents.

The following starting materials were synthesized by literature methods (or minor variations thereof), and were judged to be pure by IR spectroscopy: $[PPN]_2[Ru_3(CO)_9(CCO)]$ [11], $[PPN]_2[Os_3(CO)_9(CCO)]$ [12], and their derivatives enriched with ^{13}C at all non-PPN carbon atoms; $[Mn(CO)_3(NCMe)_3]PF_6$ [17]; $Cr(CO)_3(NCMe)_3$ [18]; $Mo(CO)_3(NCMe)_3$ [18]; and $[RhCl(CO)_2]_2$ [19]. $Ni(COD)_2$ (COD = cycloocta-1,5-diene) (Alfa Products) was used as supplied, and $Co_2(CO)_8$ (Strem) was sublimed in vacuo prior to use.

IR spectra were recorded in solution with a Mattson Alpha Centauri spectrometer using 0.1 mm path length CaF_2 solution cells. ^{13}C NMR spectra were recorded on either a JEOL FX-270 or a Varian XL-400 spectrometer operating at 67.80 and 100.577 MHz respectively. All chemical shifts are reported positive if downfield from TMS (0.00 ppm), and the ^{13}C resonance for CD_2Cl_2 (53.80 ppm) or acetone-d_6 (29.80 ppm) was used as the internal reference. $Cr(acac)_3$ (acac = acetylacetonato) was added as a shiftless relaxation agent for all ^{13}C NMR spectra. Elemental analyses were performed by Elbach Analytical Laboratories (West Germany).

Synthesis of [PPN][MnRu$_3$C(CO)$_{13}$] (I). A Schlenk flask was charged with 0.400 g (0.239 mmol) of $[PPN]_2[Ru_3(CO)_9(CCO)]$, 0.100 g (0.246 mmol) of $[Mn(CO)_3(NCMe)_3]PF_6$, and a magnetic stirbar. Acetone (20 mL) was added and the solution stirred for 2 h to give a dark red solution. The solution was evaporated to dryness, the resulting solids were extracted with 25 mL of Et_2O and the mixture was filtered. The volume of the filtrate was reduced to ca. 10 mL and pentane (40 mL) was added dropwise to the stirred solution. The resulting red microcrystals were collected by filtration, washed with pentane (5 mL) and dried in vacuo; 0.195 g isolated, 64% yield. The compound as prepared above is sufficiently pure for most purposes, as judged by IR spectroscopy. A sample for elemental analysis was recrystallized by the slow diffusion of pentane (2 mL) into an Et_2O solution (1 mL) of the cluster. Anal. Found: C, 47.03; H, 2.33; Mn, 4.27; Ru, 23.60. $C_{50}H_{30}NMnO_{13}P_2Ru_3$ calcd.: C, 47.18; H, 2.38; Mn, 4.32; Ru, 23.82%.

Synthesis of [PPN][MnOs$_3$C(CO)$_{13}$] (II). A Schlenk flask was charged with 0.100 g (0.052 mmol) of $[PPN]_2[Os_3(CO)_9(CCO)]$, 0.022 g (0.054 mmol) of $[Mn(CO)_3(NCMe)_3]PF_6$ and a magnetic stirbar. Acetone (15 mL) was added and the mixture was stirred at ca. 35 °C for 2.5 h to give a bright orange solution. The solution was evaporated to dryness, the resulting orange oil was extracted with 20 mL Et_2O, and the mixture was filtered. The volume of the filtrate was reduced to ca. 5 mL and pentane (30 mL) was added to the stirred solution. The resulting orange microcrystals were collected by filtration, washed with pentane (5 mL) and dried in vacuo; 0.065 g isolated, 82% yield. Anal. Found: C, 38.75; H, 1.91; Mn, 3.42; Os, 36.90. $C_{50}H_{30}NMnO_{13}Os_3P_2$ calcd.: C, 38.99; H, 1.96; Mn, 3.57; Os, 37.05%.

Synthesis of [PPN]$_2$[Cr$_2$Ru$_3$C(CO)$_{16}$] (III). A 0.500 g (0.299 mmol) sample of $[PPN]_2[Ru_3(CO)_9(CCO)]$ with 0.200 g (0.772 mmol) of $Cr(CO)_3(NCMe)_3$ was stirred in acetone (30 mL) for 1 h to give a very dark yellow-black solution, which was filtered through a medium-porosity frit to remove a small amount of insoluble matter. The volume of the solution was reduced to ca. 4 mL and Et_2O (40 mL) was

added slowly with stirring to give dark brown-black microcrystals, which were filtered off and washed with 10 mL of Et_2O. The product was recrystallized by the slow diffusion of 2-propanol (60 mL) into a dichloromethane solution (12 mL) of the cluster, to give black crystals which were dried in vacuo; 0.510 g isolated, 88% yield. Anal. Found: C, 54.70; H, 3.13; Cr, 5.22; Ru, 15.30. $C_{89}H_{60}N_2Cr_2O_{16}P_4Ru_3$ calcd.: C, 54.97; H, 3.11; Cr, 5.35; Ru, 15.59%.

Synthesis of [PPN]$_2$[Mo$_2$Ru$_3$C(CO)$_{16}$] (IV). A Schlenk flask was charged with 0.400 g (0.239 mmol) of $[PPN]_2[Ru_3(CO)_9(CCO)]$, 0.225 g (0.742 mmol) of $Mo(CO)_3(NCMe)_3$, and a magnetic stirbar. Acetone (20 mL) was added and the mixture was stirred for 3 h to give a dark red-black solution which was filtered through a medium porosity frit. The volume of the solution was reduced to ca. 4 mL and Et_2O (50 mL) was added slowly with stirring to give dark red-black microcrystals, which were collected by filtration and washed with 10 mL of Et_2O. The product was recrystallized by the slow diffusion of 2-propanol (50 mL) into a dichloromethane solution (10 mL) of the cluster, to give black prisms which were dried in vacuo; 0.385 g isolated, 79% yield. Anal. Found: C, 52.36; H, 2.86; Mo, 9.75; Ru, 15.10. $C_{89}H_{60}N_2Mo_2O_{16}P_4Ru_3$ calcd.: C, 52.60; H, 2.98; Mo, 9.44; Ru, 14.92%.

Synthesis of [PPN][Rh$_3$Ru$_3$C(CO)$_{15}$] (V). A 0.600 g (0.359 mmol) sample of $[PPN]_2[Ru_3(CO)_9(CCO)]$ with 0.355 g (0.913 mmol) of $[RhCl(CO)_2]_2$, was stirred with THF (25 mL) for 2.5 h to give a deep red-brown solution. The solution was evaporated to dryness, the resulting solids were extracted with 30 mL of Et_2O and the mixture was filtered to remove solid $[PPN][RhCl_2(CO)_2]$. The volume of the filtrate was reduced to 10 mL and pentane (40 mL) was added dropwise with stirring to afford tacky red-black microcrystals. The mother liquor was syringed off and discarded. The microcrystals were redissolved in 15 mL of Et_2O, the solution was filtered and pentane (40 ml) was added dropwise with stirring to give dark red microcrystals which were collected by filtration, washed with 5 mL of pentane and dried in vacuo; 0.370 g isolated, 65% yield. Anal. Found: C, 39.42; H, 2.02; Rh, 19.35; Ru, 18.90. $C_{52}H_{30}NO_{15}P_2Rh_3Ru_3$ calcd.: C, 39.46; H, 1.91; Rh, 19.51; Ru, 19.16%.

Synthesis of [PPN][Co$_3$Ru$_3$C(CO)$_{15}$] (VI). A Schlenk flask was charged with 1.00 g (0.598 mmol) of $[PPN]_2[Ru_3(CO)_9(CCO)]$, 0.670 g (1.96 mmol) of $Co_2(CO)_8$ and a magnetic stirbar. THF (30 mL) was added and the mixture was stirred for 1.5 h to give a dark yellow-brown solution. The solution was evaporated to dryness, the resulting solids were extracted with 60 mL of Et_2O and the mixture was filtered. The filtrate was evaporated to dryness and the resulting solids were extracted with 50 mL pentane. The mixture was filtered to give a dark brown pentane filtrate and a dark brown solid. The latter was re-crystallized by layering pentane (40 mL) on an Et_2O solution (15 mL) of the cluster, to give black crystals of $[PPN][Co_3Ru_3C(CO)_{15}]$; 0.335 g isolated, 43% yield. Anal. Found: C, 43.29; H, 2.15; Co, 12.20; Ru, 20.70. $C_{52}H_{30}Co_3NO_{15}P_2Ru_3$ calcd.: C, 43.05; H, 2.08; Co, 12.19; Ru, 20.90%. The pentane filtrate was evaporated to dryness to give dark-brown microcrystals of an as yet unidentified cobalt-ruthenium cluster.

Synthesis of [PPN]$_2$[Ni$_3$Ru$_3$C(CO)$_{13}$] (VII). A Schlenk flask was charged with 0.400 g (0.239 mmol) of $[PPN]_2[Ru_3(CO)_9(CCO)]$ 0.300 g (1.09 mmol) of $Ni(COD)_2$, and a magnetic stirbar. The mixture was suspended in 30 mL of THF, a reflux condenser was fitted, and a CO atmosphere was introduced. [**Caution**: at this stage

Table 1

X-ray crystal structure data for $[PPN][MnOs_3C(CO)_{13}]$ (I) and $[PPN]_2[Ni_3Ru_3(CO)_{13}C]$ (VII)

Formula	$C_{50}H_{30}MnNO_{13}Os_3P_2$	$C_{86}H_{60}N_2Ni_3O_{13}P_4Ru_3 \cdot 1.2CH_2Cl_2$
M	1540.3	(1932.6) 2034.5
Crystal size, mm	0.4×0.3×0.3	0.38×0.35×0.15
Crystal system	triclinic	monoclinic
Space group	$P\bar{1}$	$P2_1/a$
a, Å	9.219(2)	24.743(4)
b, Å	15.035(2)	13.521(2)
c, Å	18.757(5)	26.000(3)
α, deg	105.20(2)	90
β, deg	99.18(2)	91.91(1)
γ, deg	96.96(1)	90
V, Å^3	2440(2)	8693(4)
Z	2	4
d(calc), g·cm^{-3}	2.10	(1.48) 1.56
μ (Mo-K_α), cm^{-1}	81.6	14.0
radiation	Mo-K_α ($\lambda = 0.71069$ Å) graphite-monochromated	
scan type	ω–2θ	ω–2θ
2θ range, deg	4–50	4–45
unique data	8552	11909
unique data, $(I) > 3\sigma(I)$	7496	7684
no. of parameters	452	700
$R(F)$	0.029	0.056
$R_w(F)$	0.042	0.073
GOF	1.36	1.98

highly toxic $Ni(CO)_4$ is generated.] The mixture was heated quickly to reflux in a closed system whereupon the mixture rapidly turned a very dark yellow-brown. The mixture was refluxed for 25 min under a slow N_2 stream, and then evaporated to dryness. The solid was dissolved in 20 mL of dichloromethane and an overlayer of 50 mL of 2-propanol was added, producing bronze-black platelets which were washed with 5 mL of pentane before drying in vacuo; 0.390 g isolated, 84% yield. Anal. Found: C, 53.17; H, 2.99; Ni, 8.90; Ru, 15.30. $C_{86}H_{60}N_2Ni_3O_{13}P_4Ru_3$ calcd.: C, 53.44; H, 3.13; Ni, 9.11; Ru, 15.69%.

X-ray crystal structure determination of [PPN][MnOs$_3$C(CO)$_{13}$] (II). A translucent orange crystal of II suitable for X-ray diffraction was grown by slow diffusion of pentane into a 1:1 CH_2Cl_2: Et_2O solution of the cluster. The crystal was mounted on a glass fiber in air and transferred to the cold (−120 °C) stream of an Enraf-Nonius CAD4 diffractometer. A summary of the data collection is given in Table 1. Unit cell constants were determined by least-squares refinement of the setting angles of 25 unique reflections. The data were corrected for Lorentz and polarization effects. Absorption corrections were applied using the program DIFABS [20] with the transmission factors ranging from 0.74 to 1.52. A decay correction was not applied, as four standard reflections monitored periodically during data collection showed negligible variation.

All calculations were performed with the TEXSAN 4.0 software package [21] run on a MICRO VAX 3600 computer. The structure was determined by direct methods (SHELXS 86) [22] and difference Fourier techniques. High thermal displacement

Table 2

Positional parameters for [PPN][$MnOs_3C(CO)_{13}$] (II)

Atom	x	y	z
Os(1)	0.19622(2)	0.02327(1)	0.19337(1)
Os(2a)	0.50182(3)	0.07715(2)	0.19537(2)
Os(2b)	0.35165(6)	0.19144(3)	0.29296(3)
Os(3)	0.55382(2)	0.09099(1)	0.35051(1)
Mn(1a)	0.3516	0.1914	0.2930
Mn(1b)	0.5018	0.0772	0.1954
P(1)	0.1337(2)	0.3772(1)	0.68055(8)
P(2)	0.2807(2)	0.4492(1)	0.84394(8)
O(11)	0.0274(6)	0.0890(3)	0.0657(3)
O(12)	−0.0704(6)	−0.0114(4)	0.2638(3)
O(13)	0.1806(6)	−0.1826(3)	0.1165(3)
O(21)	0.5568(6)	−0.1191(3)	0.1530(3)
O(22)	0.8295(5)	0.1605(3)	0.2208(3)
O(23)	0.3854(6)	0.0732(4)	0.0340(3)
O(31)	0.4611(6)	0.0991(3)	0.4995(3)
O(32)	0.6952(6)	−0.0814(3)	0.3468(4)
O(33)	0.8437(6)	0.2348(3)	0.4124(3)
O(41)	0.1609(7)	0.1783(4)	0.4009(4)
O(42)	0.1446(5)	0.2798(3)	0.2047(3)
O(43)	0.5550(6)	0.3533(3)	0.4047(3)
O(51)	0.5449(6)	0.2928(3)	0.2076(3)
N	0.1588(5)	0.4151(3)	0.7687(3)
C(1)	0.3710(6)	0.0489(3)	0.2745(3)
C(11)	0.0883(7)	0.0614(4)	0.1118(3)
C(12)	0.0286(7)	0.0029(4)	0.2373(4)
C(13)	0.1818(7)	−0.1045(4)	0.1434(4)
C(21)	0.5366(6)	−0.0450(5)	0.1692(4)
C(22)	0.7047(7)	0.1282(4)	0.2122(4)
C(23)	0.4274(8)	0.0756(4)	0.0959(4)
C(31)	0.4994(7)	0.0970(4)	0.4439(4)
C(32)	0.6412(7)	−0.0164(4)	0.3485(4)
C(33)	0.7408(7)	0.1790(4)	0.3912(4)
C(41)	0.2356(8)	0.1833(4)	0.3589(4)
C(42)	0.2218(7)	0.2422(4)	0.2374(3)
C(43)	0.4808(8)	0.2892(4)	0.3622(3)
C(51)	0.4886(7)	0.2316(5)	0.2262(4)
C(111)	0.0201(6)	0.2627(4)	0.6468(3)
C(112)	−0.0734(7)	0.2336(4)	0.6915(4)
C(113)	−0.167(1)	0.1464(5)	0.6633(5)
C(114)	−0.1618(9)	0.0901(5)	0.5941(5)
C(115)	−0.0714(8)	0.1182(5)	0.5490(4)
C(116)	0.0197(7)	0.2053(4)	0.5755(4)
C(121)	0.0379(6)	0.4549(4)	0.6396(3)
C(122)	−0.0682(6)	0.4214(4)	0.5738(3)
C(123)	−0.1430(7)	0.4826(4)	0.5443(4)
C(124)	−0.1119(7)	0.5778(4)	0.5818(4)
C(125)	−0.0054(7)	0.6113(4)	0.6475(4)
C(126)	0.0703(7)	0.5517(4)	0.6764(4)
C(131)	0.3000(6)	0.3644(4)	0.6437(3)
C(132)	0.3562(7)	0.4244(4)	0.6051(4)
C(133)	0.4865(9)	0.4127(5)	0.5802(5)
C(134)	0.5598(9)	0.3399(5)	0.5911(5)
C(135)	0.5050(8)	0.2827(5)	0.6298(4)

Table 2 (continued)

Atom	x	y	z
C(136)	0.3766(7)	0.2939(4)	0.6563(3)
C(211)	0.2339(7)	0.3797(4)	0.9046(3)
C(212)	0.2168(7)	0.2820(4)	0.8765(4)
C(213)	0.1815(8)	0.2272(4)	0.9230(4)
C(214)	0.1626(8)	0.2683(5)	0.9941(4)
C(215)	0.1787(8)	0.3644(5)	1.0215(4)
C(216)	0.2133(7)	0.4202(4)	0.9766(3)
C(221)	0.4694(6)	0.4414(4)	0.8318(3)
C(222)	0.5341(7)	0.4976(4)	0.7934(3)
C(223)	0.6752(7)	0.4921(4)	0.7790(4)
C(224)	0.7546(8)	0.4301(5)	0.8037(4)
C(225)	0.6942(8)	0.3754(4)	0.8428(4)
C(226)	0.5496(7)	0.3788(4)	0.8565(4)
C(231)	0.2817(6)	0.5704(4)	0.8909(3)
C(232)	0.1583(7)	0.6113(4)	0.8764(3)
C(233)	0.1615(7)	0.7052(4)	0.9094(4)
C(234)	0.2882(7)	0.7591(4)	0.9575(4)
C(235)	0.4113(7)	0.7177(4)	0.9740(4)
C(236)	0.4098(7)	0.6245(4)	0.9405(3)

parameters for the sites occupied indicated a disorder placing both osmium and manganese atoms with fractional occupancy in each hinge metal site. The disorder was resolved by introducing osmium and manganese atoms in each site with refined population parameters. These converged to 73.2% osmium and 26.8% manganese at M(1), with the reverse at M(2). All non-hydrogen atoms were refined anisotropically, except for manganese and PPN carbon atoms. Hydrogen atoms were introduced without refinement into ideal positions for final calculations. A final difference map was essentially featureless, displaying two peaks (1.32, 1.44 e/Å^3) near a PPN phenyl ring. The final positional parameters are listed in Table 2.

X-ray crystal structure determination of $(PPN)_2[Ni_3Ru_3C(CO)_{13}] \cdot 1.2CH_2Cl_2$ *(VII).* A black crystal of VII was selected from those grown as described above and mounted as described for II. A summary of the data collection is given in Table 1. Unit cell constants were determined by least-squares refinement of the setting angles of 25 high angle reflections. The data were corrected for Lorentz and polarization effects. Absorption corrections were performed by DIFABS [20] with the transmission factors ranging from 0.84 to 1.09. Periodic monitoring of four standard reflections indicated no significant decay occurred during the data collection, and a correction was not applied.

Calculations were performed using software described above. The structure was determined by direct methods and difference Fourier techniques. Full-matrix least-squares refinement using anisotropic thermal parameters for the cluster anion atoms and phosphorus and nitrogen atoms of PPN cations gave an R factor of 0.070. Hydrogen atoms were included in calculated positions.

A difference Fourier map calculated at this stage revealed the presence of four peaks with heights ranging from 2.8 to 4.2 e/Å^3. As the distances between the peaks were typical of those seen between metals in butterfly clusters, it was assumed a small amount of a Ru_3Ni cluster co-crystallized with the majority anion. The atoms

Table 3

Positional parameters for $[PPN]_2[Ni_3Ru_3C(CO)_{13}]\cdot 1.2CH_2Cl_2$ (VII)

Atom	x	y	z
Ru(1)	0.77730(3)	0.14253(6)	0.28724(3)
Ru(1b)	0.7198(6)	0.145(1)	0.2112(6)
Ru(2)	0.76954(3)	0.35790(6)	0.30753(3)
Ru(2b)	0.806(1)	0.259(1)	0.2464(8)
Ru(3)	0.68816(3)	0.25439(6)	0.25073(3)
Ru(3b)	0.723(1)	0.358(2)	0.1932(9)
Ni(1)	0.76386(6)	0.3758(1)	0.20126(5)
Ni(1b)	0.729(1)	0.202(2)	0.315(1)
Ni(2)	0.77236(5)	0.2016(1)	0.18360(5)
Ni(3)	0.84779(6)	0.2809(1)	0.25741(5)
Cl(1)	0.6932(2)	0.2945(4)	0.8847(3)
Cl(2)	0.7324(2)	0.2210(3)	0.9869(2)
Cl(3)	0.2812(2)	0.2830(3)	0.5378(2)
Cl(4)	0.3062(2)	0.1827(4)	0.6346(2)
P(1)	1.0026(1)	−0.2417(2)	0.1256(1)
P(2)	1.0491(1)	−0.2394(2)	0.0211(1)
P(3)	0.0127(1)	0.2575(2)	0.6300(1)
P(4)	0.0533(1)	0.2606(2)	0.5225(1)
O(11)	0.7426(3)	−0.0527(6)	0.2404(3)
O(12)	0.8920(3)	0.0727(5)	0.3130(3)
O(13)	0.7335(4)	0.0933(8)	0.3923(4)
O(21)	0.7252(3)	0.5655(6)	0.3040(3)
O(22)	0.8831(3)	0.4441(5)	0.3239(3)
O(23)	0.7416(4)	0.3321(8)	0.4186(4)
O(31)	0.6243(3)	0.4239(5)	0.2011(3)
O(32)	0.6371(3)	0.0871(5)	0.1879(3)
O(33)	0.6276(3)	0.2352(6)	0.3500(4)
O(41)	0.9628(3)	0.2648(6)	0.2425(3)
O(42)	0.7577(4)	0.5809(7)	0.1746(4)
O(43)	0.7636(4)	0.0352(7)	0.1146(4)
O(44)	0.7873(6)	0.3297(8)	0.0953(4)
N(1)	1.0094(3)	−0.2258(5)	0.0664(3)
N(2)	0.0181(3)	0.2763(5)	0.5704(3)
C(1)	0.7694(4)	0.2689(7)	0.2456(4)
C(11)	0.7548(5)	0.0233(8)	0.2567(4)
C(12)	0.8516(4)	0.1089(7)	0.3014(4)
C(13)	0.7499(5)	0.1124(8)	0.3525(5)
C(21)	0.7414(4)	0.4845(8)	0.3049(4)
C(22)	0.8480(4)	0.3934(7)	0.3096(4)
C(23)	0.7532(5)	0.3421(9)	0.3768(5)
C(31)	0.6513(4)	0.3618(7)	0.2182(4)
C(32)	0.6581(4)	0.1503(8)	0.2099(4)
C(33)	0.6505(4)	0.2425(8)	0.3105(5)
C(41)	0.9156(5)	0.2724(8)	0.2471(4)
C(42)	0.7593(4)	0.4981(8)	0.1837(5)
C(43)	0.7678(5)	0.0994(9)	0.1421(5)
C(44)	0.7779(6)	0.309(1)	0.1379(5)
C(80)	0.731(1)	0.204(2)	0.934(1)
C(90)	0.2696(7)	0.281(1)	0.6025(7)
C(111)	0.9661(3)	−0.1377(6)	0.1500(3)
C(112)	0.9242(4)	−0.1507(7)	0.1831(4)
C(113)	0.8970(5)	−0.0658(8)	0.2013(4)

Table 3 (continued)

Atom	x	y	z
C(114)	0.9129(4)	0.0285(8)	0.1864(4)
C(115)	0.9547(4)	0.0378(8)	0.1539(4)
C(116)	0.9805(4)	−0.0428(7)	0.1354(4)
C(121)	0.9642(3)	−0.3515(6)	0.1379(3)
C(122)	0.9270(4)	−0.3847(7)	0.1017(4)
C(123)	0.8949(4)	−0.4667(8)	0.1123(4)
C(124)	0.9009(4)	−0.5147(7)	0.1592(4)
C(125)	0.9385(4)	−0.4828(7)	0.1947(4)
C(126)	0.9703(4)	−0.4000(7)	0.1850(4)
C(131)	1.0663(3)	−0.2508(6)	0.1617(3)
C(132)	1.0992(4)	−0.3317(7)	0.1547(4)
C(133)	1.1508(4)	−0.3335(7)	0.1758(4)
C(134)	1.1697(4)	−0.2559(8)	0.2053(4)
C(135)	1.1361(4)	−0.1764(8)	0.2150(4)
C(136)	1.0843(4)	−0.1728(7)	0.1928(4)
C(141)	1.0097(4)	−0.2432(6)	−0.0383(4)
C(142)	1.0261(4)	−0.2982(7)	−0.0794(4)
C(143)	0.9955(4)	−0.3015(8)	−0.1250(4)
C(144)	0.9491(5)	−0.2486(8)	−0.1294(5)
C(145)	0.9314(5)	−0.1922(8)	−0.0890(4)
C(146)	0.9615(4)	−0.1907(8)	−0.0426(4)
C(151)	1.0869(4)	−0.3521(6)	0.0246(3)
C(152)	1.0592(4)	−0.4407(7)	0.0348(4)
C(153)	1.0874(4)	−0.5283(7)	0.0411(4)
C(154)	1.1426(5)	−0.5302(8)	0.0364(4)
C(155)	1.1697(5)	−0.4459(8)	0.0244(4)
C(156)	1.1423(4)	−0.3565(8)	0.0186(4)
C(161)	1.0963(4)	−0.1392(7)	0.0175(4)
C(162)	1.1236(4)	−0.1079(7)	0.0615(4)
C(163)	1.1600(4)	−0.0275(8)	0.0619(4)
C(164)	1.1655(4)	0.0222(9)	0.0146(5)
C(165)	1.1388(5)	−0.007(1)	−0.0287(5)
C(166)	1.1034(5)	−0.0879(8)	−0.0283(4)
C(211)	−0.0265(4)	0.1484(6)	0.6421(3)
C(212)	−0.0178(4)	0.0923(7)	0.6862(4)
C(213)	−0.0509(4)	0.0106(8)	0.6951(4)
C(214)	−0.0926(5)	−0.0100(8)	0.6612(5)
C(215)	−0.1014(5)	0.0418(9)	0.6169(5)
C(216)	−0.0675(4)	0.1249(7)	0.6070(4)
C(221)	0.0766(3)	0.2456(6)	0.6646(3)
C(222)	0.0956(4)	0.3222(7)	0.6959(4)
C(223)	0.1486(4)	0.3168(8)	0.7182(4)
C(224)	0.1801(4)	0.2359(7)	0.7080(4)
C(225)	0.1605(4)	0.1601(7)	0.6776(4)
C(226)	0.1090(4)	0.1646(6)	0.6562(4)
C(231)	−0.0223(3)	0.3609(6)	0.6563(3)
C(232)	−0.0616(4)	0.3481(7)	0.6918(4)
C(233)	−0.0857(4)	0.4344(8)	0.7126(4)
C(234)	−0.0695(5)	0.5271(8)	0.6975(4)
C(235)	−0.0305(5)	0.5377(8)	0.6619(4)
C(236)	−0.0078(4)	0.4559(7)	0.6412(4)
C(241)	0.0088(3)	0.2557(6)	0.4673(3)

Table 3 (continued)

Atom	x	y	z
C(242)	0.0223(4)	0.2046(7)	0.4233(4)
C(243)	−0.0131(4)	0.2029(7)	0.3808(4)
C(244)	−0.0620(4)	0.2519(8)	0.3829(4)
C(245)	−0.0756(4)	0.3034(8)	0.4252(4)
C(246)	−0.0407(4)	0.3045(7)	0.4686(4)
C(251)	0.0999(4)	0.3609(6)	0.5147(3)
C(252)	0.1049(4)	0.4077(8)	0.4676(4)
C(253)	0.1393(5)	0.4883(8)	0.4634(5)
C(254)	0.1673(4)	0.5206(8)	0.5056(4)
C(255)	0.1641(4)	0.4754(8)	0.5537(4)
C(256)	0.1284(4)	0.3949(7)	0.5578(4)
C(261)	0.0910(4)	0.1481(6)	0.5243(3)
C(262)	0.0635(4)	0.0597(7)	0.5332(4)
C(263)	0.0904(4)	−0.0288(7)	0.5388(4)
C(264)	0.1452(5)	−0.0325(8)	0.5351(4)
C(265)	0.1724(5)	0.0549(9)	0.5246(5)
C(266)	0.1463(4)	0.1445(7)	0.5190(4)

of the cluster were refined with population parameters of 0.05 and isotropic temperature factors. It was not possible to recognize the distribution of ligands on the minority cluster.

Two partially occupied dichloromethane solvent sites were also found in the crystal lattice. They were refined with occupancy factors of 0.60. The final R factor was 0.056 ($R_w = 0.073$). The final difference map displayed two higher peaks (ca. 1.5 e/Å^3) located near the dichloromethane molecules. Final positional parameters are given in Table 3.

Results and discussion

General observations

This research provides further evidence for the utility of the trinuclear ketenylidene clusters $[M_3(CO)_9(CCO)]^{2-}$ (M = Fe, Ru, Os) in the synthesis of mixed-metal carbide clusters [7]. The range of products that may be formed from the ketenylidene cluster $[Ru_3(CO)_9(CCO)]^{2-}$ is illustrated in Scheme 1. The most successful cluster building reactions occur when the transition-metal reagents are electrophilic in nature. This can be accomplished with complexes containing either labile ligands [as in $M(CO)_3(NCMe)_3$ (M = Cr, Mo) complexes] or coordinatively unsaturated metal centers [as in $Rh_2Cl_2(CO)_4$]. IR spectroscopy provided a convenient method for monitoring the cluster building reactions. The main band in the CO stretching region is an excellent indicator of cluster charge, with ca. 50 cm^{-1} increase in ν(CO) occurring for each decrease in negative charge (Table 4).

Isolated clusters have been characterized by elemental analyses, IR spectroscopy, ^{13}C NMR spectroscopy, and for the clusters $[PPN][MnOs_3C(CO)_{13}]$ (II) and $[PPN]_2[Ni_3Ru_3C(CO)_{13}]$ (VI) by single-crystal X-ray diffraction studies. Excellent ^{13}C NMR spectra were obtained for all clusters (Table 5), as $[PPN]_2[Ru_3(CO)_9(CCO)]$ can be readily enriched to 30% ^{13}C for all non-PPN carbon atoms

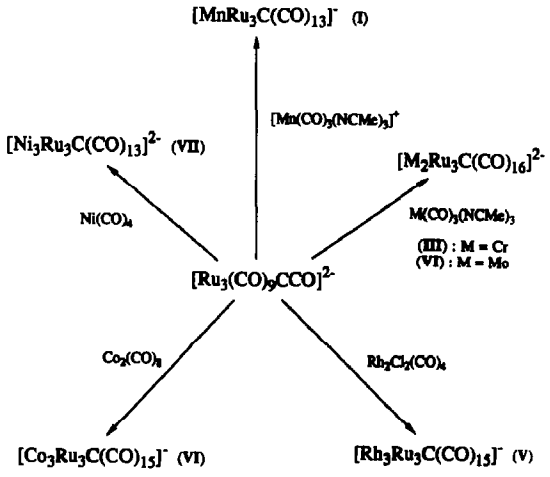

Scheme 1

[11]. Mixed-metal carbide clusters prepared from this ketenylidene cluster are enriched with ^{13}C at both the carbide atom and at all of the carbonyl ligands, as a result of isotopic scrambling between the ketenylidene carbonyl ligands and the heterometal carbonyls. The resonance for the carbide ligand was found, in all cases, to be far downfield from the carbonyl ligands, in the range 331.1–472.3 ppm.

Synthesis of mixed-metal ruthenium and osmium carbide clusters

The reactions between the ketenylidene clusters $[M_3(CO)_9(CCO)]^{2-}$ (M = Ru or Os) and $[Mn(CO)_3(NCMe)_3]^+$ proceed smoothly with the addition of a single $Mn(CO)_3^+$ fragment in both cases to afford the diethyl ether-soluble monoanions $[MnM_3C(CO)_{13}]^-$. In contrast, the reactions between $[Ru_3(CO)_9(CCO)]^{2-}$ and $M(CO)_3(NCMe)_3$ (M = Cr, Mo) result in the addition of two heterometal fragments to afford the pentametal clusters $[M_2Ru_3C(CO)_{16}]^{2-}$ (M = Cr, Mo). No further reactions to produce hexanuclear clusters were observed at room temperature. The

Table 4

IR CO stretching frequencies for heterometallic ruthenium carbide clusters [a]

Compound	Medium	ν(CO), cm^{-1}
[PPN][$MnRu_3C(CO)_{13}$] (I)	Et_2O	2068vw, 2023vs, 1998m, 1988m, 1964w, 1945w, 1909vw, br, 1862w, br.
[PPN][$MnOs_3C(CO)_{13}$] (II)	Et_2O	2071vw, 2025vs, 2004w, 1985s, 1959w, 1945w, 1863vw, br.
[PPN]$_2$[$Cr_2Ru_3C(CO)_{16}$] (III)	CH_2Cl_2	2039vw, 1999s, 1956s, sh, 1954vs, 1879w, 1845w, 1781w.
[PPN]$_2$[$Mo_2Ru_3C(CO)_{16}$] (IV)	CH_2Cl_2	2044vw, 1991vs, 1973vs, 1952m, sh, 1886w, br, 1875vw, sh, 1798w, br.
[PPN][$Rh_3Ru_3C(CO)_{15}$] (V)	Et_2O	2054vw, 2033w, sh, 2017vs, 2003m, sh, 1962w, 1886w, br.
[PPN][$Co_3Ru_3C(CO)_{15}$] (VI)	Et_2O	2063vw, 2013vs, 1976vw, 1854w, br.
[PPN]$_2$[$Ni_3Ru_3C(CO)_{13}$] (VII)	CH_2Cl_2	2020vw, 1976vs, 1896w, br, 1818w, br.

[a] Legend: vs = very strong; s = strong; m = medium; w = weak; vw = very weak; sh = shoulder; br = broad.

Table 5

^{13}C NMR data for heterometallic carbide clusters [a]

Compound	Temp. (°C)	^{13}C NMR data (ppm)
[PPN][$MnRu_3C(CO)_{13}$]	25	420.8(1), 225.4(4), 200.9(6), 199.9(2), 193.3(1).
[PPN][$MnRu_3C(CO)_{13}$]	−90	419.1(1) [t, J(C–C) = 116 Hz], 229.2(1), 227.8(2), 215.9(1), 205.2(2) [t, J(C–C) = 16 Hz], 200.0(2), 199.3(2), 198.6(2), 193.1(1).
[PPN][$MnOs_3C(CO)_{13}$]	25	331.1(1), 218.0 br(4), 183.6 br(6), 179.5(2), 173.7(1).
[PPN][$MnOs_3C(CO)_{13}$]	−90	330.2(1) [t, J(C–C) = 16 Hz], 224.8(2), 210.8(1), 210.3(1), 191.0(2) [t, J(C–C) = 16 Hz], 181.0(2), 180.5(2), 179.7(2), 173.8(1).
[PPN]$_2$[$Cr_2Ru_3C(CO)_{16}$] [b]	48	472.3(1), 223.6(16).
[PPN]$_2$[$Cr_2Ru_3C(CO)_{16}$]	−90	466.8(1), 245.8(2), 229.4(2), 218.9(10), 205.0(2).
[PPN]$_2$[$Mo_2Ru_3C(CO)_{16}$]	10	464.1(1), 220.7(16).
[PPN]$_2$[$Mo_2Ru_3C(CO)_{16}$]	−90	463.8(1), 225.6(10), 211.8(6).
[PPN][$Rh_3Ru_3C(CO)_{15}$]	10	452.2(1) [q, J(Rh–C) = 23 Hz], 204.5(15) [q, J(Rh–C) = 12 Hz].
[PPN][$Rh_3Ru_3C(CO)_{15}$]	−90	452.6(1) [q, J(Rh–C) = 22 Hz], 205.8(15) br.
[PPN]$_2$[$Ni_3Ru_3C(CO)_{13}$]	−50	416.2(1), 242.5(1), 211.8(9), 198.9(3).
[PPN][$Co_3Ru_3C(CO)_{15}$]	−30	455.2, 453.5, 214.5 br.
[PPN][$Co_3Ru_3C(CO)_{15}$]	−90	455.2, 453.4, 246.9, 245.0 br, 240.5, 212.2 br, 202.0 br, 199.9, 197.0, 196.2, 194.8.

[a] Resonances due to PPN cation are omitted; the numbers in parentheses are the relative intensities; spectra recorded in CD_2Cl_2 solution, unless noted. [b] Spectra recorded in acetone-d_6.

attempted isolation of a four-metal $[CrRu_3C(CO)_{13}]^{2-}$ species using one equivalent of $Cr(CO)_3(NCMe)_3$, high dilution techniques and low (−78 °C) reaction temperature was unsuccessful. In all cases, a mixture of $[Cr_2Ru_3C(CO)_{16}]^{2-}$ and $[Ru_3(CO)_9(CCO)]^{2-}$ formed, as judged by IR spectroscopy.

The reaction of $[Ru_3(CO)_9(CCO)]^{2-}$ with an excess of $Ni(CO)_4$ in refluxing THF affords the hexanuclear cluster $[Ni_3Ru_3C(CO)_{13}]^{2-}$. Interestingly, the formation of this cluster can be reversed by stirring a dichloromethane solution of the cluster under an atmosphere of carbon monoxide (a large excess) at ca. 40 °C for 1 h. This behavior is analogous to that displayed by the clusters $[MFe_3C(CO)_{13}]^{2-}$ (M = Cr, W), which may be formed from $[Fe_3(CO)_9(CCO)]^{2-}$ and $M(CO)_3(NCR)_3$, but revert to starting materials when the heterometallic clusters are dissolved in acetonitrile [7b]. We find that stirring a dichloromethane solution of the [PPN]$_2$[$Ni_3Ru_3C(CO)_{13}$] product (prepared using ^{13}C enriched ketenylidene) under 40 torr of ^{13}CO for 2 h at ca. 35 °C leads to enrichment of the carbonyl ligands with ^{13}CO, with only negligible decomposition to [PPN]$_2$[$Ru_3(CO)_9(CCO)$] and $Ni(CO)_4$, as shown by IR spectroscopy.

The reaction between $[Ru_3(CO)_9(CCO)]^{2-}$ and $[RhCl(CO)_2]_2$ produced $[Rh_3Ru_3C(CO)_{15}]^-$ as the sole cluster product. Attempts to isolate intermediate tetra- or pentanuclear RhRu clusters using stoichiometric quantities of $[RhCl(CO)_2]_2$ were not successful. This is in contrast to the $[Fe_3(CO)_9(CCO)]^{2-}$ system, where tetra- and pentanuclear RhFe clusters were isolable [7]. Other syntheses in this work also indicate that such tetranuclear species are extremely reactive toward the further addition of metal fragments.

We have reported previously [23] that the iron ketenylidene cluster $[Fe_3(CO)_9(CCO)]^{2-}$ undergoes a metal substitution reaction with $Co_2(CO)_8$, affording the mixed-metal ketenylidene $[CoFe_2(CO)_9(CCO)]^-$. This, together with related metal substitution reactions [24] prompted us to investigate the reaction of $[Ru_3(CO)_9(CCO)]^{2-}$ with $Co_2(CO)_8$, but cluster building to yield $[Co_3Ru_3C(CO)_{15}]^-$ was observed rather than metal substitution. An additional unidentified pentane-soluble cobalt-ruthenium containing cluster is produced. Judging from ^{13}C NMR, this compound may not contain a carbide moiety. It is possible that in the reaction of $[Fe_3(CO)_9CCO]^{2-}$ with $Co_2(CO)_8$ a transient tetra- or higher nuclearity FeCo carbide cluster is formed, which then fragments to generate the mixed-metal FeCo ketenylidene. The difference in behavior between the iron and ruthenium ketenylidenes is presumably a result of the increased metal–metal bond strength with the ruthenium complexes.

X-ray crystal structure of [PPN][$MnOs_3C(CO)_{13}$] (II)

As depicted in Fig. 1, the metal core of the cluster anion $[MnOs_3C(CO)_{13}]^-$ adopts a butterfly configuration, as has been observed for most other previously characterized tetranuclear carbide clusters [1,7].

Overall, the cluster anion bears a very strong resemblance to the $Ru_4C(CO)_{13}$ cluster described by Lewis and co-workers [25]. The carbide ligand is located between the wingtip metals and centered over the hinge metal–metal bond in a μ_4-bonding fashion. As with heterometallic butterfly carbide clusters derived from the iron ketenylidene $[Fe_3(CO)_9(CCO)]^{2-}$ [7], the heterometal appears exclusively on the hinge. The crystal shows disorder however, resulting in partial occupation of the two hinge metal positions, labeled M(1) and M(2), by both osmium and manganese. This type of disorder has been observed in previous studies on heterometallic iron carbide clusters [7]. Least-squares refinement of population parameters

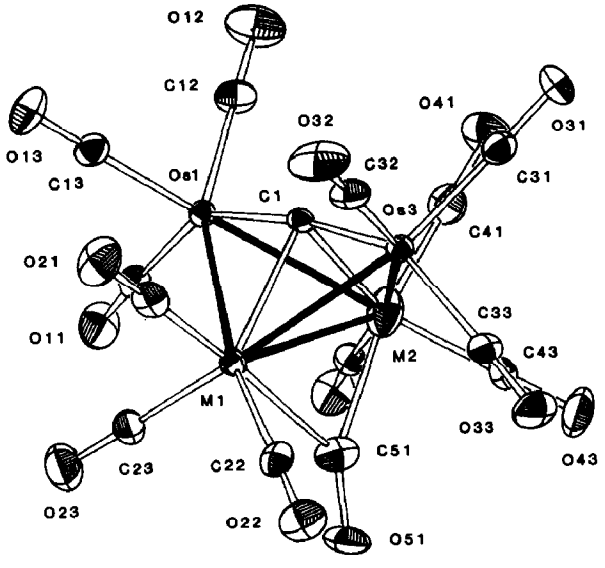

Fig. 1. ORTEP diagram for the cluster anion of [PPN][$MnOs_3C(CO)_{13}$] (II) showing the atom labeling scheme. Thermal ellipsoids are drawn at the 35% probability level.

Table 6

Selected bond distances (Å) and angles (°) for [PPN][$MnOs_3C(CO)_{13}$] (II)

Bond distances

Os(1)–M(1)	2.8271(7)	M(1)–C(21)	1.855(7)	C(12)–O(12)	1.131(8)
Os(1)–M(2)	2.7797(9)	M(1)–C(22)	1.877(7)	C(13)–O(13)	1.147(7)
Os(1)–C(1)	1.954(5)	M(1)–C(23)	1.875(7)	C(21)–O(21)	1.121(8)
Os(3)–M(1)	2.8203(9)	M(1)–C(51)	2.264(7)	C(22)–O(22)	1.162(8)
Os(3)–M(2)	2.7956(7)	Os(3)–C(31)	1.881(7)	C(23)–O(23)	1.155(8)
Os(3)–C(1)	1.943(5)	Os(3)–C(32)	1.884(6)	C(31)–O(31)	1.146(8)
M(1)–M(2)	2.8205(8)	Os(3)–C(33)	1.950(6)	C(32)–O(32)	1.145(8)
M(1)–C(1)	2.149(5)	M(2)–C(41)	1.778(7)	C(33)–O(33)	1.128(7)
M(2)–C(1)	2.114(5)	M(2)–C(42)	1.828(6)	C(41)–O(41)	1.136(8)
Os(1)–C(11)	1.943(7)	M(2)–C(43)	1.830(6)	C(42)–O(42)	1.160(7)
Os(1)–C(12)	1.894(6)	M(2)–C(51)	2.060(7)	C(43)–O(43)	1.138(7)
Os(1)–C(13)	1.882(6)	C(11)–O(11)	1.151(8)	C(51)–O(51)	1.162(7)

Bond angles

Os(1)–M(2)–M(1)	60.63(2)	C(41)–M(2)–C(51)	167.6(3)
Os(1)–M(2)–Os(3)	88.39(2)	C(42)–M(2)–C(43)	106.8(3)
Os(1)–M(1)–M(2)	58.97(2)	C(42)–M(2)–C(51)	80.7(3)
Os(1)–M(1)–Os(3)	86.97(2)	C(43)–M(2)–C(51)	79.2(3)
Os(3)–M(1)–M(2)	59.42(2)	C(1)–Os(1)–C(11)	147.9(2)
Os(3)–M(2)–M(1)	60.29(2)	C(1)–Os(1)–C(12)	106.0(2)
M(1)–Os(1)–M(2)	60.40(2)	C(1)–Os(1)–C(13)	103.6(2)
M(1)–Os(3)–M(2)	60.29(2)	C(1)–M(1)–C(21)	91.4(2)
Os(1)–C(1)–M(1)	87.0(2)	C(1)–M(1)–C(22)	129.2(2)
Os(1)–C(1)–M(2)	86.1(2)	C(1)–M(1)–C(23)	125.9(2)
Os(1)–C(1)–Os(3)	171.4(3)	C(1)–M(1)–C(51)	94.1(2)
Os(3)–C(1)–M(1)	87.0(2)	C(1)–Os(3)–C(31)	106.7(2)
Os(3)–C(1)–M(2)	87.0(2)	C(1)–Os(3)–C(32)	105.6(3)
M(1)–C(1)–M(2)	82.9(2)	C(1)–Os(3)–C(33)	147.9(2)
Os(1)–M(1)–C(1)	43.7(1)	C(1)–M(2)–C(41)	90.6(2)
Os(1)–M(2)–C(1)	44.5(1)	C(1)–M(2)–C(42)	127.8(2)
Os(3)–M(1)–C(1)	43.5(1)	C(1)–M(2)–C(43)	125.0(3)
Os(3)–M(2)–C(1)	44.0(1)	C(1)–M(2)–C(51)	101.4(2)
M(1)–M(2)–C(1)	49.1(1)	M(1)–C(51)–M(2)	81.3(2)
M(2)–M(1)–C(1)	48.0(1)	Os(1)–C(11)–O(11)	176.3(5)
C(11)–Os(1)–C(12)	95.1(3)	Os(1)–C(12)–O(12)	178.2(6)
C(11)–Os(1)–C(13)	99.0(3)	Os(1)–C(13)–O(13)	175.5(6)
C(12)–Os(1)–C(13)	93.5(3)	M(1)–C(21)–O(21)	179.4(6)
C(21)–M(1)–C(22)	93.3(2)	M(1)–C(22)–O(22)	178.1(6)
C(21)–M(1)–C(23)	94.5(3)	M(1)–C(23)–O(23)	177.7(6)
C(21)–M(1)–C(51)	173.0(2)	M(1)–C(51)–O(51)	132.0(6)
C(22)–M(1)–C(23)	104.0(3)	Os(3)–C(31)–O(31)	177.5(6)
C(22)–M(1)–C(51)	79.9(2)	Os(3)–C(32)–O(32)	179.3(6)
C(23)–M(1)–C(51)	85.8(3)	Os(3)–C(33)–O(33)	174.6(6)
C(31)–Os(3)–C(32)	93.4(3)	M(2)–C(41)–O(41)	179.6(7)
C(31)–Os(3)–C(33)	96.1(3)	M(2)–C(42)–O(42)	175.7(5)
C(32)–Os(3)–C(33)	95.0(3)	M(2)–C(43)–O(43)	175.9(6)
C(41)–M(2)–C(42)	94.3(3)	M(2)–C(51)–O(51)	146.7(6)
C(41)–M(2)–C(43)	91.5(3)		

indicate that M(1) is 73.2% osmium and 26.8% manganese, and vice versa for M(2).

Each metal atom bears three terminal carbonyls [Os–C(av) = 1.91; M(1)–C(av) = 1.87; M(2)–C(av) = 1.81; C–O(av) = 1.14 Å]. It is noteworthy that the Os(1)–

C(11) and Os(3)–C(33) bond distances (Table 6) are longer than the other metal–carbonyl bond distances of these metals. This bond lengthening presumably arises from steric interactions between these two carbonyls and carbonyls on the hinge metals, and also occurs in the previously characterized $[RhFe_3(CO)_{12}C]^-$ cluster [7a]. The hinge osmium and manganese atoms of II are asymmetrically bridged by a carbonyl ligand [M(1)–C(51) = 2.264(7); M(2)–C(51) = 2.060(7); C–O = 1.162(7) Å]. The average metal–metal distance is 2.81 Å, and the M(2)–Os(1) and M(2)–Os(3) bond distances are notably shorter [2.7956(7) and 2.7797(9) Å] than the M(1)–Os(1) and M(1)–Os(3) bond distances [2.8271(7) and 2.8203(8) Å], consistent with M(2) having greater Mn occupation than M(1). The wingtip osmium–carbide bond lengths are 1.954(5) and 1.943(5) Å, compared to 2.05(2) Å for the wingtip Os–carbide distance in the open butterfly carbide cluster $H_2PtOs_3C(CO)_{10}(PCy_3)$ [10]. These data indicate that the wingtip Os–carbide bonding in $[MnOs_3C(CO)_{13}]^-$ is somewhat stronger than that in $H_2PtOs_3C(CO)_{10}(PCy_3)$. The Os(1)–C(1)–Os(3) bond angle of 171.4(3)° for $[MnOs_3C(CO)_{13}]^-$ is very similar to the corresponding Ru–C–Ru angle of 171.2(3)° in $Ru_4C(CO)_{13}$ [25]. The hinge metal–carbide M(1)–C and M(2)–C bond distances in $[MnOs_3C(CO)_{13}]^-$ of 2.149(5) and 2.114(5) Å demonstrate that the carbide ligand is bonded more strongly to the wingtip metals than to the hinge metals. This has been observed primarily in other butterfly carbide clusters, and has been described by a theoretical study [26] on tetrairon butterfly carbides. Computed overlap populations for the carbide to wingtip-metal orbitals were found to be greater than for the carbide to hinge iron orbitals, this being largely due to the extensive σ overlap between the carbide p_y and cluster b_2 orbitals. Optimization of this σ overlap, together with important π interactions, favors a more linear wingtip metal-carbide-wingtip metal configuration, with a concomitant stronger bonding of the carbide ligand to the wingtip metals than the hinge metals.

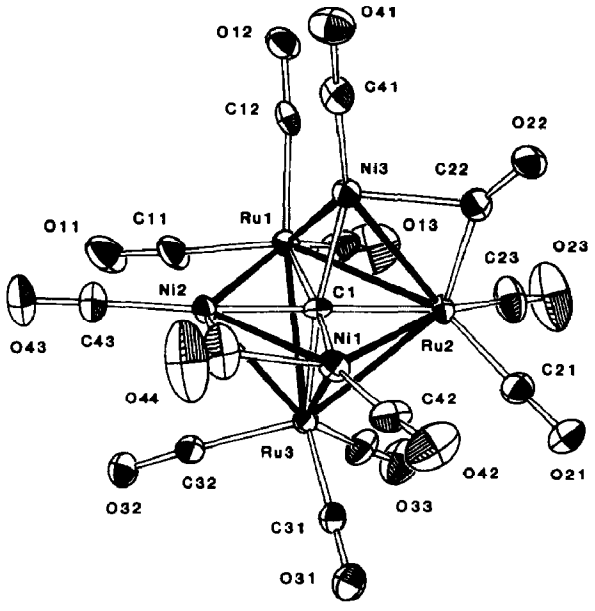

Fig. 2. ORTEP diagram for the cluster anion of $[PPN]_2[Ni_3Ru_3C(CO)_{13}]$ (VII) showing the atom labeling scheme. Thermal ellipsoids are drawn at the 35% probability level.

X-ray crystal structure of $[PPN]_2[Ni_3Ru_3C(CO)_{13}] \cdot 1.2CH_2Cl_2$ *(VII)*

This cluster, with six metal atoms and 86 valence electrons, would be expected to form an octahedral framework about an interstitial μ_6 carbide ligand [27]. As illustrated in Fig. 2 however, the cluster anion exhibits unusual metal–metal bonding, with one very short bond of 2.409(2) Å (Ni(1)–Ni(2)) and two open non-bonded distances, (Ni(1)–Ni(3) and Ni(2)–Ni(3)), resulting in a distorted (opened) octahedral metal framework. There is a remarkable range in the lengths of the metal–metal and metal–carbide bond lengths, from 2.409(2) (Ni(1)–Ni(2)) to 2.967(1) Å (Ru(1)–Ru(2)) and 1.85(1) (Ni(1)–C(1)) to 2.03(1) Å (Ru(1–3)–C(1)) respectively. The PPN cations were unexceptional. Pertinent bond lengths and angles are listed in Table 7.

Co-crystallized with VII in the selected crystal was a small fraction of another cluster compound, apparently a $[Ru_3NiC]^{2-}$ butterfly, Fig. 3. Unfortunately, the disposition of the carbide and carbonyl ligands could not be discerned, but it appears from intermetallic distances that a nickel atom may appear at a wingtip position rather than on the hinge. Although the butterfly has not been isolated and characterized spectroscopically, such a cluster is presumed to be an intermediate in the formation of VII from $[Ru_3(CO)_9CCO]^{2-}$ or to result from minor decomposition of VII in solution. It is possible to view VII alternately as a butterfly, with a nickel atom on a wingtip and the other two added as RC(O)Ni(CO) fragments about the carbide. These fragments lie out of the hinge-carbide plane, producing the opened octahedron.

A similar distortion was noted by Johnson, Lewis and co-workers in the crystal structure of $[Fe_4Au_2C(CO)_{12}(PEt_3)_2]$ [28]. One can formally view this cluster as the product derived from the addition of two $Au(PR_3)^+$ cations about the carbide ligand of $[Fe_4C(CO)_{12}]^{2-}$, although a different route was utilized in the synthesis. The cluster crystallized with a twist in the Au–Au vector compared to the hinge, placing one gold atom closer to each wingtip than the other [2.770(1) vs. 2.999(2) Å]. The resulting distortion in the octahedron destroys two possible mirror planes, but the cluster retains a two-fold axis through the center of the hinge and the carbide. This arrangement was rationalized by assuming each gold atom was placed to form a strong σ bond to the carbide and to maximize the overlap of an empty p orbital with a filled orbital on the proximal wingtip metal. Noting the isoelectronic natures of $(Et_3P)Au$ and RC(O)Ni(CO), one might speculate that similar bonding considerations are responsible for the opened structure of VII, but their importance here is not clear. Indeed, ^{13}C NMR data (discussed below) suggest the closure of the metal framework of VII to form an octahedron is actually quite facile.

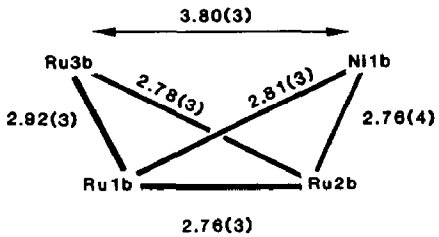

Fig. 3. A diagram showing distances (Å) between the partially occupied butterfly sites imposed on the lattice of VII.

Table 7

Selected bond distances (Å) and angles (°) for $(PPN)_2[Ni_3Ru_3C(CO)_{13}]$ (VII)

Bond distances

Ru(1)–Ru(2)	2.967(1)	Ni(2)–C(1)	1.86(1)	Ni(2)–C(44)	1.88(1)
Ru(1)–Ru(3)	2.813(1)	Ni(3)–C(1)	1.96(1)	C(11)–O(11)	1.15(1)
Ru(1)–Ni(2)	2.809(2)	Ru(1)–C(11)	1.87(1)	C(12)–O(12)	1.14(1)
Ru(1)–Ni(3)	2.689(2)	Ru(1)–C(12)	1.92(1)	C(13)–O(13)	1.15(2)
Ru(2)–Ru(3)	2.828(1)	Ru(1)–C(13)	1.89(1)	C(21)–O(21)	1.17(1)
Ru(2)–Ni(1)	2.772(2)	Ru(2)–C(21)	1.85(1)	C(22)–O(22)	1.16(1)
Ru(2)–Ni(3)	2.588(2)	Ru(2)–C(22)	2.00(1)	C(23)–O(23)	1.14(2)
Ru(3)–Ni(1)	2.831(2)	Ni(3)–C(22)	2.04(1)	C(31)–O(31)	1.15(1)
Ru(3)–Ni(2)	2.853(2)	Ru(2)–C(23)	1.87(1)	C(32)–O(32)	1.14(1)
Ni(1)–Ni(2)	2.409(2)	Ru(3)–C(31)	1.90(1)	C(33)–O(33)	1.19(1)
Ni(1)···Ni(3)	2.809(2)	Ru(3)–C(32)	1.90(1)	C(41)–O(41)	1.18(1)
Ni(2)···Ni(3)	2.842(2)	Ru(3)–C(33)	1.85(1)	C(42)–O(42)	1.15(1)
Ru(1)–C(1)	2.03(1)	Ni(3)–C(41)	1.71(1)	C(43)–O(43)	1.13(2)
Ru(2)–C(1)	2.01(1)	Ni(1)–C(42)	1.72(1)	C(44)–O(44)	1.17(2)
Ru(3)–C(1)	2.03(1)	Ni(2)–C(43)	1.75(1)		
Ni(1)–C(1)	1.85(1)	Ni(1)–C(44)	1.92(1)		

Bond angles

Ru(1)–Ru(2)–Ru(3)	58.03(3)	Ru(3)–C(31)–O(31)	172.9(9)
Ru(1)–Ru(2)–Ni(1)	84.83(4)	Ru(3)–C(32)–O(32)	174.9(9)
Ru(1)–Ru(2)–Ni(3)	57.43(4)	Ru(3)–C(33)–O(33)	178(1)
Ru(1)–Ru(3)–Ru(2)	63.46(3)	Ru(3)–Ni(1)–Ni(2)	65.38(5)
Ru(1)–Ru(3)–Ni(1)	86.66(4)	Ru(3)–Ni(2)–Ni(1)	64.46(5)
Ru(1)–Ru(3)–Ni(2)	59.44(3)	Ni(1)–Ru(2)–Ni(3)	63.09(5)
Ru(1)–Ni(2)–Ni(1)	95.54(6)	Ni(1)–Ru(3)–Ni(2)	50.16(4)
Ru(1)–Ni(2)–Ru(3)	59.58(4)	Ni(2)–Ru(1)–Ni(3)	62.19(4)
Ru(1)–Ni(3)–Ru(2)	68.38(4)	Ru(1)–C(1)–Ru(2)	94.6(4)
Ru(2)–Ru(1)–Ni(2)	83.70(4)	Ru(1)–C(1)–Ru(3)	87.8(4)
Ru(2)–Ru(1)–Ni(3)	54.20(4)	Ru(1)–C(1)–Ni(1)	173.5(6)
Ru(2)–Ru(1)–Ru(3)	58.50(3)	Ru(1)–C(1)–Ni(2)	92.5(4)
Ru(2)–Ru(3)–Ni(1)	58.67(4)	Ru(1)–C(1)–Ni(3)	84.7(4)
Ru(2)–Ru(3)–Ni(2)	85.49(4)	Ru(2)–C(1)–Ru(3)	88.9(4)
Ru(2)–Ni(1)–Ru(3)	60.60(4)	Ru(2)–C(1)–Ni(1)	91.7(4)
Ru(2)–Ni(1)–Ni(2)	95.90(6)	Ru(2)–C(1)–Ni(2)	172.2(6)
Ru(3)–Ru(1)–Ni(2)	60.98(4)	Ru(2)–C(1)–Ni(3)	81.4(4)
Ru(3)–Ru(1)–Ni(3)	92.15(4)	Ru(3)–C(1)–Ni(1)	93.7(4)
Ru(3)–Ru(2)–Ni(1)	60.74(4)	Ru(3)–C(1)–Ni(2)	94.5(4)
Ru(3)–Ru(2)–Ni(3)	93.99(4)	Ru(3)–C(1)–Ni(3)	167.2(6)
Ni(1)–C(44)–Ni(2)	78.6(6)	Ni(1)–C(1)–Ni(2)	81.1(4)
Ru(2)–C(22)–Ni(3)	79.7(4)	Ni(1)–C(1)–Ni(3)	94.9(5)
Ru(1)–C(11)–O(11)	176(1)	Ni(2)–C(1)–Ni(3)	96.2(5)
Ru(1)–C(12)–O(12)	167.3(9)	Ni(3)–C(41)–O(41)	176.7(9)
Ru(1)–C(13)–O(13)	179(1)	Ni(1)–C(42)–O(42)	176(1)
Ru(2)–C(21)–O(21)	177.9(9)	Ni(2)–C(43)–O(43)	178(1)
Ru(2)–C(22)–O(22)	150.2(8)	Ni(1)–C(44)–O(44)	138(1)
Ni(3)–C(22)–O(22)	129.9(8)	Ni(2)–C(44)–O(44)	143(1)
Ru(2)–C(23)–O(23)	178(1)		

Stone and co-workers also note that platinum-group metal complexes often violate the EAN formalism by adopting 16-electron configurations, and thus hetero-metallic clusters containing several platinum group metal centers may not adhere to

the structural predictions of the polyhedral skeletal electron pair theory [10b]. Homometallic platinum-group clusters frequently adopt structures that violate conventional PSEPT [29,30]. Therefore, the structure of the 86-electron cluster $[Co_3Pt_3C(\mu\text{-}H)(\mu\text{-}CO)_4(CO)_5(P^iPr_3)_2]$ was also shown to be an opened octahedron by X-ray crystallography, with one long non-bonding distance of 3.260(1) Å between adjacent platinum vertices.

An opened square pyramidal Ni_2Ru_3 cluster, $(CpNi)_2Ru_3(CO)_9(\mu_5\text{-}PPh)$ has also been reported [31]. The two nickel atoms occupy adjacent positions on the basal plane, but are not bonded [d(Ni–Ni) = 3.461(3) Å]. The framework also contains two $Ru(CO)_3$ fragments on the plane, which is capped on either side by a third $Ru(CO)_3$ vertex and the bridging phosphinidene ligand.

Variable-temperature ^{13}C NMR studies of [PPN][$MnM_3C(CO)_{13}$] (M = Ru, Os)

The ^{13}C NMR spectra of [PPN][$MnM_3C(CO)_{13}$] (M = Ru, Os) at −80 °C (Table 5) are completely consistent with the solid-state structure of the $[MnOs_3C(CO)_{13}]^-$ cluster, Fig. 1. The strong similarity between the spectra for $[MnRu_3C(CO)_{13}]^-$ and $[MnOs_3C(CO)_{13}]^-$, Fig. 4, indicates that these clusters have the same structure in solution, and have C_s symmetry. Both molecules contain a mirror plane which passes through the carbide, hinge metals and the bridging carbonyl. In agreement with the solid state structure of II, Mn must therefore occupy a hinge position in both clusters in solution. Nine resonances are predicted and observed in the low temperature (−80 °C) spectra of both clusters. For I and II, one resonance is far

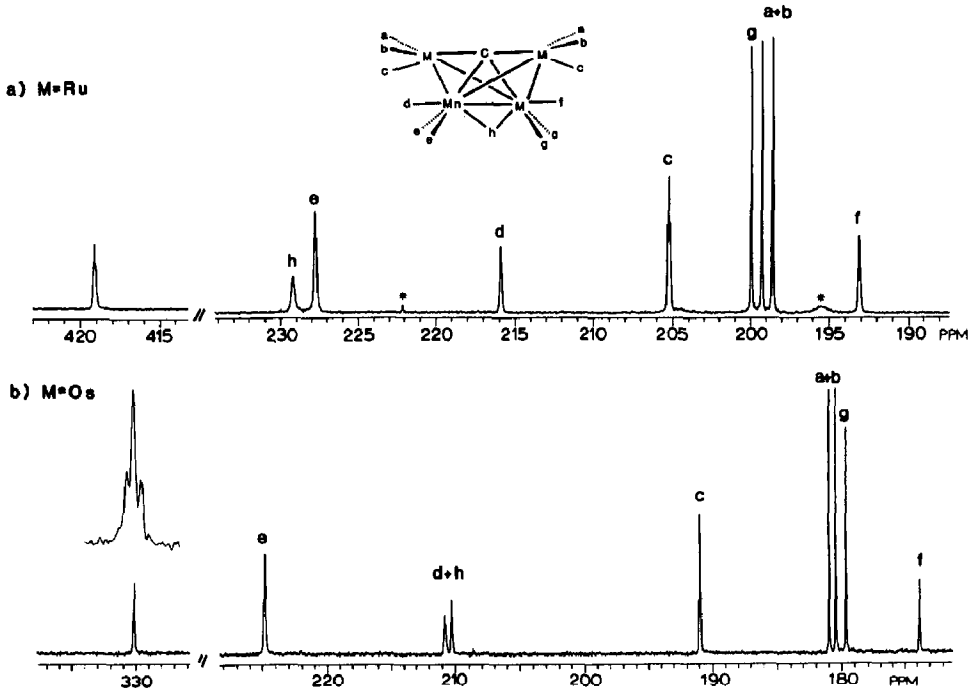

Fig. 4. Carbonyl and carbide regions of the $^{13}C\{^1H\}$ NMR spectra (100.577 MHz) of (a) [PPN]-[$MnRu_3C(CO)_{13}$] and (b) [PPN][$MnOs_3C(CO)_{13}$] in CD_2Cl_2 at −80 °C with proposed carbonyl peak assignments. The peaks marked * are due to minor impurities.

downfield from the others, at 419.1 and 330.2 ppm for I and II respectively, these being readily assigned to the carbide ligand.

The remaining eight resonances for I and II are in the region typical for carbonyl ligands, in the approximate range 170–230 ppm. Examination of the variable temperature data indicates three groups of CO ligands. For I, variable temperature behavior is as follows. Peaks at 229.2, 227.8 and 215.9 ppm in the intensity ratio 1 : 2 : 1 are assigned to the bridging carbonyl, the two symmetry-related manganese carbonyls and the unique manganese carbonyl respectively. When the system is warmed, these resonances broaden, collapse and then coalesce to a singlet at 225.2 ppm. The relative assignment of these peaks is based upon the assumption that the chemical shifts of the terminal manganese carbonyls will not differ significantly between I and II. In the case of I this allows the trivial assignment of the bridging carbonyl as the peak at 229.2 ppm. However, for II, a definitive assignment is not possible, due to near coincidence of the bridging carbonyl and the unique manganese carbonyl. The second set of resonances is composed of the peaks at 200.0 and 193.1 ppm, which broaden simultaneously on warming to room temperature. These are assigned to the carbonyl ligands bonded to the hinge ruthenium atom. The third set of CO resonances consists of three peaks of intensity 2, at 205.1, 199.3 and 198.6 ppm, and these are assigned to the carbonyls on the symmetry-related wing-tip ruthenium atoms. On warming, these resonances simultaneously broaden, collapse and then form a single peak in the room-temperature spectrum at 200.9 ppm. The variable-temperature behavior displayed by the manganese–osmium cluster II is identical to I.

A striking feature of the low temperature spectra of I and II is the 16 Hz coupling that is observed between the carbide ligand and two wingtip carbonyls. As illustrated in Fig. 4, this results in a five-line resonance for the carbide. This arises from overlap of resonances due to the various possible isotopomers, which are $^{12}CO–^{13}C(carbide)–^{12}CO$, $^{13}CO–^{13}C(carbide)–^{12}CO$, and $^{13}CO–^{13}C(carbide)–^{13}CO$ and give rise to singlet, doublet and triplet resonances respectively. Coupling of this type has not been observed previously in tetranuclear butterfly carbide clusters, but it is likely to represent simple two-bond coupling. Another possibility, direct bonding interaction between the carbide ligand and two wingtip carbonyls, seems unlikely. The structure determination performed on II indicates that two opposite wingtip carbonyls in *endo* environments form C–Os–C(carbide) angles of 147.9(2)°. All other carbide–osmium–carbonyl carbon angles are more perpendicular, ranging from 90.6(2) to 129.2(2)°. If the structure for the solid is retained in solution, the coupling may arise from the *endo* C–Os–CO array. The magnitude of the observed carbon–carbon coupling is consistent with the strong bonding interaction which is postulated to occur between the wingtip metals and the carbide atom in four-metal butterfly clusters of this type [26]. At higher temperatures, no coupling is discernible. This is primarily a result of an increase in intra-metal carbonyl site exchange.

Variable-temperature ^{13}C NMR studies of $[PPN]_2[Cr_2Ru_3C(CO)_{16}]$ (III) and $[PPN]_2[Mo_2Ru_3C(CO)_{16}]$ (IV)

The variable-temperature ^{13}C NMR spectra of $[PPN]_2[M_2Ru_3C(CO)_{16}]$ (M = Cr or Mo) have been recorded to −90 °C (Table 5). However, these spectra give relatively little information regarding the structure of these clusters, since they remain rather fluxional, even at −90 °C. For both complexes however, only a single

carbide resonance was observed, at ca. 468 and 464 ppm for $[Cr_2Ru_3C(CO)_{16}]^{2-}$ and $[Mo_2Ru_3C(CO)_{16}]^{2-}$ respectively, indicating the presence of only a single carbide-containing species in each case.

At room temperature the ^{13}C NMR spectrum of $[PPN]_2[Cr_2Ru_3C(CO)_{16}]$ (III) in acetone-d_6 consists of two peaks at 467 and 222.3 ppm, assigned to the carbide and carbonyl groups respectively. These resonances are broad at this temperature, but on warming to 48°C both sharpen. Furthermore, on cooling to −90°C the carbide and carbonyl resonances respectively sharpen and broaden, and at −90°C, the latter is replaced by four peaks with integrated ratios 2:2:10:2. The downfield carbonyl resonance at 245.8 ppm may be attributed to bridging carbonyls, and the cluster apparently contains a mirror-plane, but no other structural information may be ascertained from this spectrum. Electron-counting considerations indicates this cluster and $[Mo_2Ru_3C(CO)_{16}]^{2-}$ will have square-pyramidal metal cores, but it is not possible to umambiguously assign the positions of the heterometals. The ^{13}C NMR spectrum of $[PPN]_2[Mo_2Ru_3C(CO)_{16}]$ at 10°C displays a single carbonyl peak at 220.7 ppm. On cooling to −90°C, this peak is replaced by two somewhat broader peaks at 225.6 and 211.8 ppm. Unlike the Cr analogue however, the resonance for the Mo–Ru carbide remains sharp throughout the range +25 to −90°C. The origin of the variable temperature behavior of the carbide resonance of $[Cr_2Ru_3C(CO)_{16}]^{2-}$ is not clear at present. As described earlier for the $[MnM_3C(CO)_{13}]^-$ (M = Ru, Os) cluster, it is possible that carbon spin–spin coupling may account for this broadening. Alternately, a mechanism of carbonyl exchange involving the carbide ligand, similar to that proposed for a tetrairon cluster [1], might be responsible.

Variable-temperature ^{13}C NMR study of $[PPN][Rh_3Ru_3C(CO)_{15}]$ (V)

The room-temperature ^{13}C NMR spectrum of $[PPN][Rh_3Ru_3C(CO)_{15}]$ (V) is consistent with its formulation as a trirhodium carbide. The cluster is highly fluxional at room temperature, and a single carbonyl resonance is observed as a quartet with $J(Rh–C) = 12$ Hz due to spin–spin coupling to three rhodium centers (^{103}Rh, $I = 1/2$, 100% abundance). The carbide resonance is also a quartet with $J(Rh–C) = 23$ Hz. This value is similar to that of 19 Hz observed previously for $[Rh_3Fe_3C(CO)_{15}]^-$ [7b]. On cooling to −90°C the carbide resonance remains as a sharp quartet but the carbonyl resonance broadens considerably, and the molecule is still highly fluxional at this temperature. The structure of the cluster is presumably either a trigonal-antiprism [as in $Rh_3Fe_3C(CO)_{15}]^-$ or an octahedron. Interestingly, the spectrum of $[PPN][Rh_3Ru_3C(CO)_{15}]$ at 10°C also shows, in addition to the major carbonyl resonance, a minor quartet resonance centered at 203.15 ppm with $J(Rh–C) = 12$ Hz. The intensity ratio of minor to major carbonyl resonances is 1:10. The minor resonance also arises via coupling of the carbonyls to three rhodium centers, but the identity of the complex is uncertain, since only a single carbide resonance was observable under the spectral conditions employed. One possible explanation, however, is that the minor carbonyl resonance is attributable to a different isomer of $[Rh_3Ru_3C(CO)_{13}]^-$ with overlapping carbide resonances.

Variable-temperature ^{13}C NMR study of $[PPN][Co_3Ru_3C(CO)_{15}]$ (VI)

The ^{13}C NMR spectrum of $[PPN][Co_3Ru_3C(CO)_{15}]$ at −30°C displays a broad peak centered at 214.5 ppm, indicating that the cluster is highly fluxional at this

temperature. However, two carbide resonances are observed, at 455.2 and 453.4 ppm with approximate relative intensities 1 : 6. The IR spectrum of this ^{13}C-enriched material was satisfactory, and did not give any indication of possible impurities. The nature of the minor compound is unknown but it may be due to a different isomer of $[Co_3Ru_3C(CO)_{15}]^-$ being present, as suggested for the related $[Rh_3Ru_3C(CO)_{15}]^-$ cluster which shows similar behavior. The low temperature (−90 °C) spectrum of $[Co_3Ru_3C(CO)_{15}]^-$ compound is somewhat complex. Peaks at 246.9, 245.0(br), and 240.5 ppm are attributable to bridging carbonyls, broad peaks at 212.2 and 202.0 ppm to cobalt carbonyls, and peaks at 199.9, 197.0, 196.2 and 194.8 ppm to ruthenium carbonyls. Due to the presence of two isomers in solution, unfortunately no assignment could be made for structure in solution.

Variable-temperature ^{13}C NMR study of $[PPN]_2[Ni_3Ru_3C(CO)_{13}]$ (VII)

The ^{13}C NMR spectrum of $[PPN]_2[Ni_3Ru_3C(CO)_{13}]$ (VII) at −50 °C, Table 5, consists of a carbide resonance at 416.2 ppm and three carbonyl resonances at 242.5, 211.8 and 198.9 ppm of relative intensities 1 : 9 : 3. Line broadening of the two smaller carbonyl peaks is observed on warming to −20 °C, indicating slow exchange of these carbonyls occurs above −50 °C. No other temperature effects were observed.

These data provide little structural information, and are difficult to reconcile with the previously described structure determination, but comparison with the spectrum of $[Ni_3Fe_3(CO)_{13}C]^{2-}$ is useful [7b]. The spectrum of the iron analog, recorded at −90 °C in CD_2Cl_2, displays a similar pattern, with a carbide resonance at 435.1 ppm and three carbonyl resonances in a 1 : 9 : 3 intensity ratio at 243.4, 226.2 and 197.3 ppm. Assuming the clusters are isostructural, one can assign the largest resonance in each spectrum to terminal iron and ruthenium carbonyls on the basis of the downfield shift observed on replacing ruthenium with iron. The single carbonyl resonating furthest downfield would therefore be a bridge between two nickel atoms, and the remaining resonance is assigned to three equivalent terminal nickel carbonyls. This latter absorption lies in a fairly narrow range of chemical shifts observed for terminal carbonyls on many mononuclear nickel complexes [32]. All carbonyls are inequivalent for the structure of VII in the solid state, so it is necessary to account for the single resonances observed in solution for the nickel carbonyls and for nine ruthenium carbonyls.

As mentioned previously, this cluster has the 86 valence electrons necessary to form a closed octahedron, yet in the solid state an open structure is adopted. We propose that the open structure can isomerize to a closed octahedron in solution. This could be accomplished by closing the Ni_3 face, forming bonds from Ni(3) to Ni(1) and Ni(2). The carbonyl bridging Ni(1) and Ni(2) shifts to a face-capping position about all three nickels, and the Ru(2)–Ni(3) bridging carbonyl assumes a terminal position on Ru(2).

The postulated closed structure may be present as either stable symmetric species or as a transient species in a fluxional process which reverts back to the open framework characteristic of the solid state. This process would scramble inequivalent metal positions on the reopened structure, and thus account for the observed ^{13}C NMR spectrum. The data do not permit us to unequivocally distinguish between these possibilities.

Conclusions

The anionic ketenylidene clusters $[M_3(CO)_9(CCO)]^{2-}$ (M = Ru, Os) are versatile precursors for the synthesis of tetra-, penta-, and hexanuclear heterometallic carbide clusters. The tetranuclear clusters have a butterfly metal arrangement with the heterometal on the hinge. In some cases, spin–spin coupling between carbonyl ligands and the carbide center was observable in the variable-temperature ^{13}C NMR spectra. The $[Ni_3Ru_3C(CO)_{13}]^{2-}$ cluster adopts an open octahedral metal framework that appears to isomerize in solution on the basis of ^{13}C NMR spectroscopic data.

Acknowledgements

We are grateful for support of this work by the NSF through the Synthetic Organometallic Program, Grant CHE-8942133. We also thank the Department of Energy Grant DE-FG02-86ER13640 and the Johnson Matthey Company for a loan of osmium tetraoxide.

References

1 J.S. Bradley, Adv. Organomet. Chem., 22 (1983) 1 and references therein.
2 E.H. Brage, L.F. Dahl, W. Hubel, D.L. Wampler, J. Am. Chem. Soc., 84 (1962) 4633.
3 K.H. Whitmire, J. Coord. Chem., 17 (1988) 95 and references therein.
4 M.D. Vargas, J.N. Nicholls, Adv. Inorg. Chem. Radiochem., 30 (1986) 123.
5 M.H. Chisholm, J. Organomet. Chem., 334 (1987) 77.
6 J.D. Corbett, Pure Appl. Chem., 56 (1984) 1527.
7 (a) J.A. Hriljac, P.N. Swepston, D.F. Shriver, Organometallics, 4 (1985) 158; (b) J.A. Hriljac, E.M. Holt, D.F. Shriver, Inorg. Chem., 26 (1987) 2943.
8 (a) P. Chini, B.T. Heaton, Top. Curr. Chem., 71 (1977) 1; (b) R. Adams in D.F. Shriver, H.D. Kaesz and R.D. Adams (Eds.), Chemistry of Metal Cluster Complexes, VCH, New York, 1990, p. 121.
9 M. Tachikawa, A.C. Sievert, E.L. Muetterties, M.R. Thompson, C.S. Day, V.W. Day, J. Am. Chem. Soc., 102 (1980) 1725.
10 (a) L.J. Farrugia, A.D. Miles, F.G.A. Stone, J. Chem. Soc., Dalton Trans., (1985) 2437; (b) J.C. Jeffery, M.J. Parrott, F.G.A. Stone, J. Organomet. Chem., 382 (1990) 225.
11 M.J. Sailor, C.P. Brock, D.F. Shriver, J. Am. Chem. Soc., 109 (1987) 6015.
12 M.J. Went, M.J. Sailor, P.L. Bogdan, C.P. Brock, D.F. Shriver, J. Am. Chem. Soc., 109 (1987) 6023.
13 B.F.G. Johnson, J. Lewis, W.J.H. Nelson, J.N. Nicholls, M.D. Vargas, J. Organomet. Chem., 249 (1983) 255.
14 S.R. Bunkhall, H.D. Holden, B.F.G. Johnson, J. Lewis, G.N. Pain, P.R. Raithby, M.J. Taylor, J. Chem. Soc., Chem. Commun., (1984) 25.
15 D.L. Davies, J.C. Jeffery, D. Miguel, P. Sherwood, F.G.A. Stone, J. Chem. Soc., Chem. Commun., (1987) 454.
16 (a) D.F. Shriver, M.A. Drezdzon, The Manipulation of Air-Sensitive Compounds, 2nd Ed., Wiley, New York, 1986; (b) H.C. Brown, Organic Synthesis via Boranes, Wiley, New York, 1975.
17 D. Drew, D.J. Darensbourg, M.Y. Darensbourg, Inorg. Chem., 14 (1975) 1579.
18 D.P. Tate, W.R. Knipple, J.M. Augl, Inorg. Chem., 1 (1962) 433.
19 J.A. McCleverty, G. Wilkinson, Inorg. Synth., 8 (1966) 211.
20 N. Walker, D. Stuart, Acta Cryst. A, 39 (1983) 158.
21 P.N. Swepston, TEXSAN, Version 4.0, the TEXRAY Structure Analysis Program Package, Molecular Structure Corporation, College Station, TX, 1987.
22 G.M. Sheldrick, SHELXS 86; a program for crystal structure determination, University of Göttingen, F.R.G., 1986.
23 S. Ching, E.M. Holt, J.W. Kolis, D.F. Shriver, Organometallics, 7 (1988) 892.

24 H. Beurich, R. Blumhofer, H. Vahrenkamp, Chem. Ber., 115 (1982) 2409; R.A. Epstein, H.W. Withers, G.L. Geoffroy, Inorg. Chem., 18 (1979) 942; A. Ceriotti, G. Longoni, R.D. Pergola, B.T. Heaton, D.O. Smith, J. Chem. Soc., Dalton Trans., (1983) 1433.
25 A.G. Cowie, B.F.G. Johnson, J. Lewis, P.R. Raithby, J. Organomet. Chem., 306 (1986) C63.
26 S. Harris, J.S. Bradley, Organometallics, 3 (1984) 1086.
27 (a) J.W. Lauher, J. Am. Chem. Soc., 100 (1978) 5305; (b) D.M.P. Mingos, Adv. Organomet. Chem., 15 (1977) 1; (c) K. Wade, Adv. Inorg. Chem. Radiochem., 18 (1975) 1.
28 B.F.G. Johnson, D.A. Kaner, J. Lewis, P.R. Raithby, M.J. Rosales, J. Organomet. Chem., 231 (1982) C59.
29 D.J. Wales, D.M.P. Mingos, L. Zhenyang, Inorg. Chem., 28 (1989) 2754.
30 Evans and Mingos have suggested a modified PSEP theory for correlating the structure of homometallic platinum clusters with electron count. (a) D.G. Evans, D.M.P. Mingos, J. Organomet. Chem., 240 (1982) 321; (b) idem, ibid., 251 (1983) C13.
31 M. Lanfranchi, A. Tiripicchio, E. Sappa, S.A. MacLaughlin, A.J. Carty, J. Chem. Soc., Chem. Commun., (1982) 538.
32 B.E. Mann, B.F. Taylor, ^{13}C NMR Data for Organometallic Compounds, Academic Press, London, 1981.